Theoretical Mechanism Studies on the Enantioselectivity of *aza*-MBH-type Reaction of Nitroalkene to N-tosylimine Catalyzed by Thiourea-tertiary Amine

Nan Lu,* Huatian Wang,†,* and Yangping Wang

College of Chemistry and Material Science, Shandong Agricultural University, Taian City 271018, Shandong Prov., P.R. China
E-mail: lun@sdau.edu.cn
†*College of Forestry, Shandong Agricultural University, Taian City 271018, Shandong Prov., P.R. China*
E-mail: wanght@sdau.edu.cn

The enantioselective *aza*-Morita Baylis Hillman reaction of nitroalkene and N-tosylimine catalyzed by thiourea-tertiary amine has been investigated using density functional theory. Enantioselectivity is dominated by the cooperative effect of non-covalent and weak covalent interactions imposed by different units of catalyst. As Lewis base, the tertiary amine unit activates nitroalkene *via* weak covalent bond. The weak covalent interaction orients the reaction in a major path with smaller variations of this bond. The aromatic ring unit activates N-tosylimine *via* π-π stacking. The non-covalent interaction selects the major path with smaller changes of the efficient packing areas. Thiourea unit donates more compact H-bonded network for species of the major path. The calculated ee value in xylene solution phase (97.6%) is much higher than that in *N,N*-Dimethylformamide (27.2%). Our conclusion is also supported by NBO analysis.

Key Words : Lewis base, Weak covalent interaction, π-π stacking, Non-covalent interaction, Density functional theory

Introduction

Carbon-carbon bond formation *via* the functionalization of sp^3 and sp^2 C-H bonds is considered to be central parts in synthetic chemistry.[1] Devoting to the case of sp^2 C-H bonds, *aza*-Morita Baylis Hillman (*aza*-MBH) reaction is known to involve a coupling reaction of activated electron-deficient alkenes with various carbon electrophiles catalyzed by Lewis base.[2-5] Typically as an important tandem reaction, this method is capable of providing α-functionalized alkenes starting from simple materials with minimal production of waste.[6] Moreover, the catalytic *aza*-MBH-type reaction is of great potential in the synthesis of optically active amines.[7]

A wide range of organocatalysts have emerged for *aza*-MBH-type reaction, such as 1,4-diazabicyclo[2.2.2]octane (DABCO), 1,5-diazabicyclo[4.3.0]non-5-ene (DBU), and phosphine.[8-11] Recently, Pohmakotr has described an asymmetric MBH reaction catalyzed by tributylphosphine in the presence of phenol.[12] Verkade isolated the MBH type adducts employing P(PhCH₂NCH₂CH₂)₃N as an efficient catalyst.[13] Without Lewis acid or base, the α-acylvinyl anion equivalents could still undergo highly selective addition to imines generating α-substituted *aza*-MBH-type adducts.[14] However, in the reaction of allenyl ketone and aldehyde,[15] DABCO and 4-Dimethylaminopyridine (DMAP) could not lead to the desired products.[16] Challenge also exists in the organocatalytic enantioselective version employing nitro-activated olefins as nucleophiles.

A breakthrough solving this problem was Xu's enantioselective *aza*-MBH-type reaction catalyzed by thiourea-tertiary amine.[17] To the best of our knowledge there is no report about mechanistic study at present. In the synthesis of β-nitro-γ-enamines,[18] how are the two substrates activated by catalyst? In screening of catalysts, why is the best enantio-selectivity obtained with the structure incorporating aromatic ring, thiourea and tertiary amine units? To draw a detailed picture of the intrinsic mechanism for this experimental work, we herein perform an in-depth theoretical study[19,20] of its mechanism based on density functional theory (DFT) calculations[21,22] as well as previous experimental data. Generally, the hybrid function is accurate enough to describe complexes with H bonds. DFT method is also well-documented for the rationalization and quantitative prediction of stereoselectivity in organocatalysis.[23]
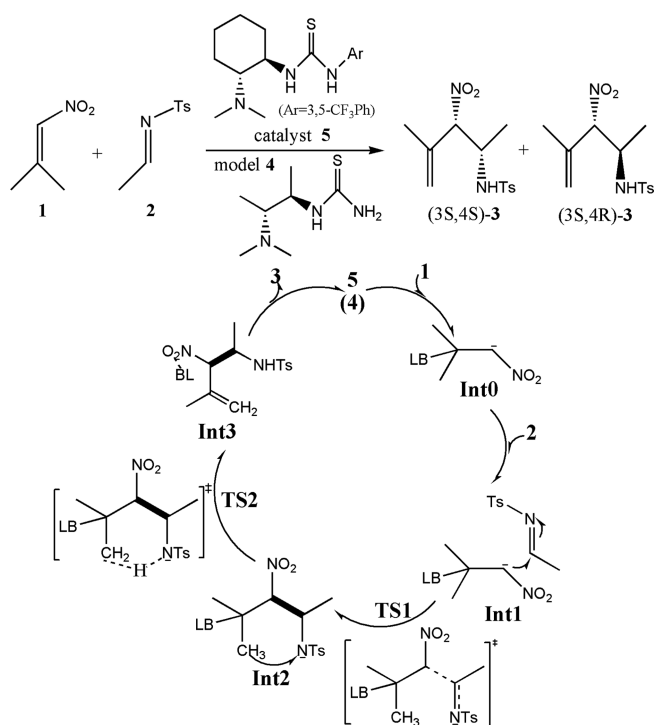
Computational Details

All calculations were carried out using DFT as implemented in Gaussian 09.[24] We chose to use the popular B3LYP functional, which includes Becke's three-parameter hybrid functional combined with the LeeYangParr correction for correlation.[25-27] All structures studied in this paper were fully optimized with the 6-31G(d,p) basis set. Frequencies were analyzed at the same level to characterize the nature of stationary points (energy minima or first-order saddle-points) and to provide free energies at 298.15 K and 1 atm pressure, which include entropic contributions by considering the vibrations, rotations, and translations of the structures. When necessary, the intrinsic reaction coordinate (IRC) calculations were performed to verify the right connections among a transition state and its forward, backward minima.

To consider the solvent effect on reaction, single-point

calculations with self-consistent reaction field[28-30] based on the integral equation formalism polarizable continuum model (IEFPCM)[31] with UAKS radii and cavity-dispersion-solvent-structure terms in Truhlar and co-workers' SMD solvation model[32] for xylene and *N,N*-dimethylformamide (DMF) were applied for all gas-phase optimized structures at B3LYP/ 6-311++G(d,p) and MP2/6-311++G(d,p) levels.[33,34] For all cited energies, ZPE corrections were taken into account.The basis set superposition error (BSSE) corrections for species were estimated using the counterpoise method.[35] In order to evaluate the direction and magnitude of the donor–acceptor interactions for some stationary points, natural bond orbital (NBO) analysis was also performed.[36,37]

Results and Discussion

The mechanism we suggest for the catalytic *aza*-MBH-type reaction is outlined in Scheme 1. As Lewis base, the catalyst activates nitroalkene **1** by tertiary amino group to enhance the nucleophilicity of the initial binary complex **Int0**. The nucleophilic addition of **Int0** to N-tosylimine **2** gives **Int2**. Then the proton transfers from methyl of **1** to the electronegative N of **2**, which is followed by the generation of β-nitro-β-enamine **3** and the regeneration of catalyst. In research of the reaction process, the catalyst **5** in experiment[17] was simulated by model **4** bearing critical elements for catalysis, namely thiourea and tertiary amine.[23] The tosyl group of **2** was also substituted with acetyl (**2'**) for simplification. Symbols "**s**" and "**a**" were used to distinguish species of two paths leading to isomers (3*S*,4*S*)-**3** and (3*S*,4*R*)-**3**, respectively (Fig. 1). When it comes to the enantioselec-
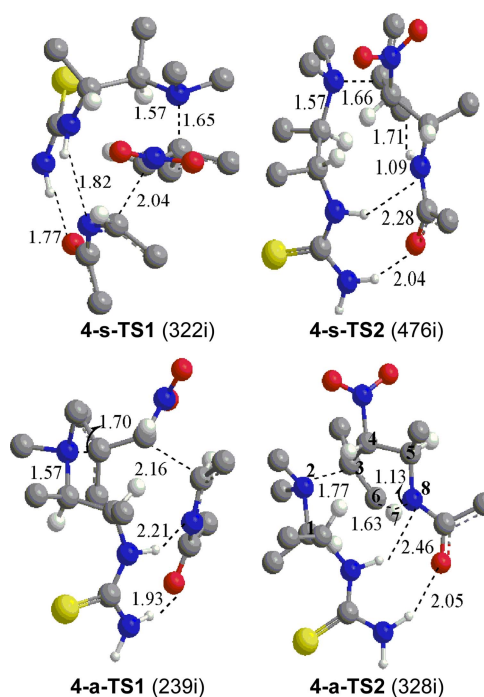

Figure 1. Optimized geometries (bond length in Å) of four transition states in two steps of the *aza*-MBH-type reaction with catalyst model **4** (Hydrogen atoms of methyl and on the ring are omitted for clarity; blue, red, gray, yellow and white balls represent N, O, C, S and H atoms, respectively; the imaginary frequency (cm⁻¹) of transition states are in parentheses.).
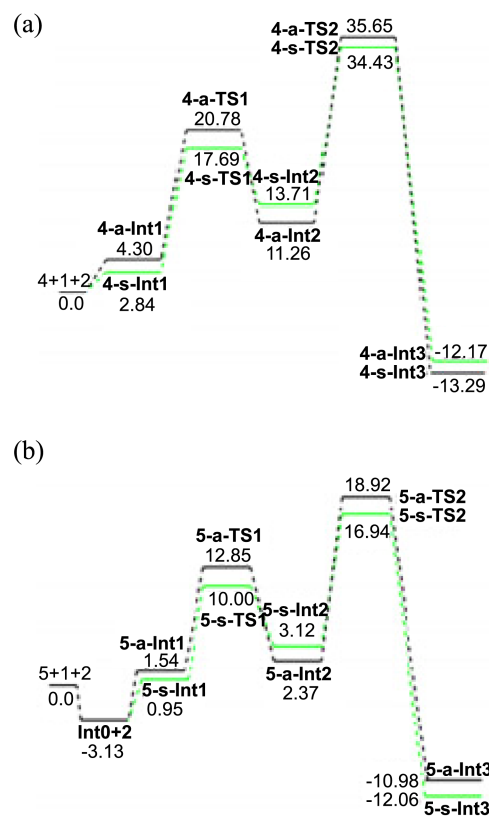

Figure 2. Relative electronic energy profiles (kcal mol⁻¹) of **s** path (green) and **a** path (black) in the *aza*-MBH-type reaction with (a) catalyst **4** and (b) catalyst **5** in solution phase of xylene.

Scheme 1. Proposed mechanistic rationale of thiourea-tertiary amine-catalyzed enantioselective *aza*-MBH-type reaction.

tivity, real system with full catalyst **5** was taken into account (Fig. 3). Key atoms involved in bond cleavage and formation are numbered in structures of Figure 1 and Figure 3. Relative electronic energy profiles of the reaction in solution phase are depicted in Figure 2.

Reaction with Model Catalyst. In **s** path of step1, the nucleophilic addition of **Int0** to N-acetylimine **2'** takes place *via* **4-s-TS1** from a pre-reactive complex **4-s-Int1** yielding an active intermediate **4-s-Int2**. This step is endothermic by 10.87 kcal mol^{-1} with a barrier of 14.85 kcal mol^{-1}. The H bonds between N, O atoms of **2'** and thiourea of **4** in **4-s-Int1** (1.84, 1.92 Å) are stronger than those of **4-a-Int1** (2.01, 2.20 Å). The case is inversed in **4-s-Int2** (1.72, 1.89 Å) and **4-a-Int2** (1.68, 1.71 Å), which advocates the higher energy of **4-s-Int2** (13.71 kcal mol^{-1}) than **4-a-Int2** (11.26 kcal mol^{-1}). Although the distance between N2 and C3 (N2···C3) exceeds the length of normal single C-N bond (1.47-1.55 Å),[38] it denotes one type of weak covalent interaction between the catalyst and nitroalkene. The length of N2-C3 is nearly the same in corresponding intermediates. The discrepancy appears in two transition states (**4-s-TS1**, 1.65 Å; **4-a-TS1**, 1.70 Å). The transition vector of **4-s-TS1** (322i cm^{-1}) corresponds to the formation of C4-C5 bond (2.04 Å). In **4-a-TS1** (239i cm^{-1}), lengths of C4-C5 bond is 2.16 Å. Along with two H bonds of **4-s-TS1** (1.77, 1.82 Å) shorter than those of **4-a-TS1** (1.93, 2.21 Å), the desired C-C bond formation is more readily accessible in **s** path than in **a** path.

The proton transfer proceeds *via* **TS2** from **Int2** yielding a stable intermediate **Int3**. Two paths are both exothermic (**s**: −25.88; **a**: −24.21 kcal mol^{-1}) with energy barriers of 20.72 (**s**) and 24.39 (**a**) kcal mol^{-1}, respectively. Obviously, the proton transfer is rate-limiting step of the catalytic *aza*-MBH-type reaction. The transition vector of **TS2** corresponds to the formation of N8-H7 bond (**s**: 1.09 Å; **a**: 1.13 Å) and cleavage of C6-H7 bond (**s**: 1.71 Å; **a**: 1.63 Å). The interaction between **4** and **1** in **4-a-TS2** (1.77 Å) is weaker than that of **4-s-TS2** (1.66 Å). Moreover the H bonds mentioned above in **4-a-TS2** (2.05, 2.46 Å) are longer than those of **4-s-TS2** (2.04, 2.28 Å). Evidently, **4-s-TS2** (476i cm^{-1}) is more favorable than **4-a-TS2** (328i cm^{-1}) leading to the (3S,4S)-**3**.

To verify the reliability of B3LYP method, we carried out single-point calculations for species in rate-limiting step of

Table 1. Relative electronic energy (kcal mol^{-1}) of species in rate-limiting step2 with catalyst **4** at two different levels

Species	B3LYP/6-311++G(d,p)		MP2/6-311++G(d,p)	
	[a]E (a.u.)	[b]ΔE	[a]E (a.u.)	[b]ΔE
4-s-Int2	-1486.9015	12.43	-1486.9078	10.32
4-s-TS2	-1486.8685	31.40	-1486.8786	28.61
[c]Ea(**s**)		18.97		18.29
4-a-Int2	-1486.9054	10.01	-1486.9119	6.95
4-a-TS2	-1486.8665	32.67	-1486.8771	28.79
[c]Ea(**a**)		22.66		21.84

[a]Real energies (a.u.). [b]Relative energy considering ZPE and BSSE corrections. [c]Activation energy barrier.

5-s-TS1 (323i)   HOMO of **5-s-TS1**

5-a-TS1 (217i)   HOMO of **5-a-TS1**

5-s-TS2 (945i)   HOMO of **5-s-TS2**

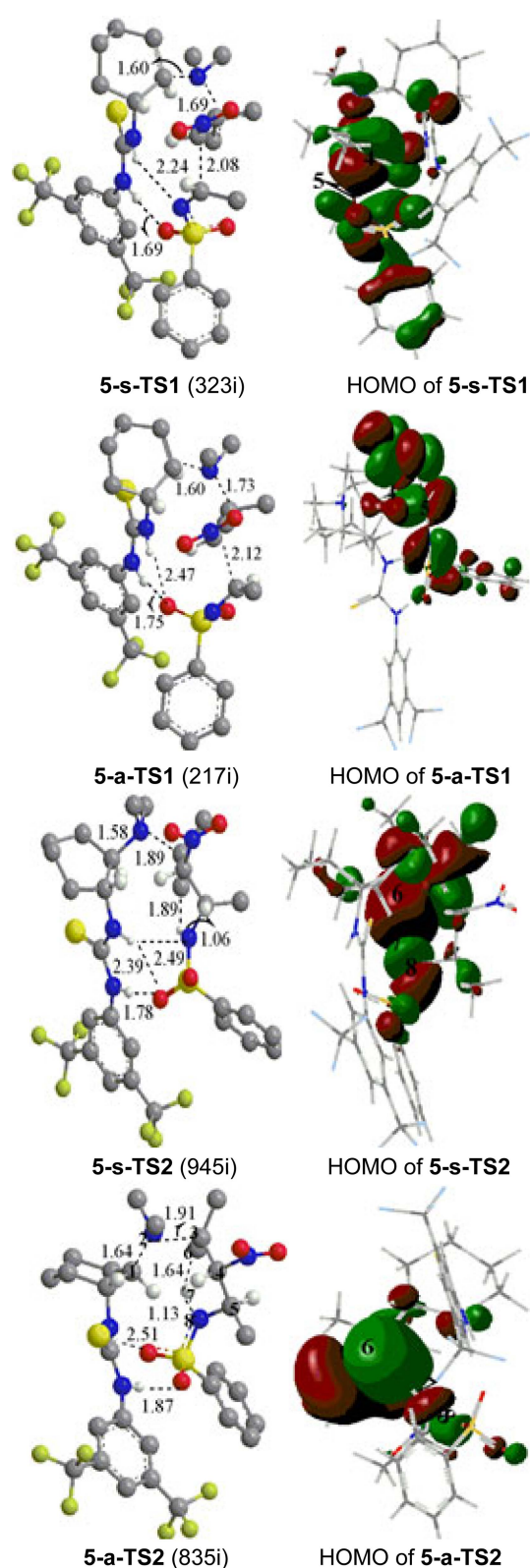**5-a-TS2** (835i)   HOMO of **5-a-TS2**

Figure 3. Optimized geometries (bond length in) and HOMO of four transition states in two steps of the *aza*-MBH-type reaction with full catalyst **5** (In left column, hydrogen atoms of methyl and on the ring are omitted for clarity; blue, red, gray, yellow, white and kelly balls represent N, O, C, S, H and F atoms, respectively; the imaginary frequency (cm^{-1}) of transition states are in parentheses. In right column, different colors are used to identify the phase of the wave functions).

two paths with catalyst **4** at two different levels (Table 1). Compared with the case of B3LYP, both electronic energy and relative energy of species with MP2 method are lowered at different degrees. The energy barriers of two paths decrease by 0.68 (**s**) and 0.82 (**a**) kcal mol^{-1}, respectively. This difference is small so that its influence could almost be omitted. In the following analysis, B3LYP method will be applied to replace the time-consuming MP2 method.

The detailed mechanism is made clear with the help of model catalyst **4**. After the activation of nitroalkene by tertiary amino group of catalyst, the catalytic cycle consists of nucleophilic addition and proton transfer. Step2 is rate-limiting.

Real System with Full Catalyst.

Structural Characteristic of Transition States: The optimized geometries of transition states in real system with full catalyst **5** are illustrated in the left column of Figure 3. In step1, lengths of the forming C4-C5 bond in **5-s-TS1** and **5-a-TS1** are 2.08 and 2.12 Å, respectively. The distances of N2-C3 and two H bonds are 1.69, 1.69, 2.24 Å in **5-s-TS1** and 1.73, 1.75, 2.47 Å in **5-a-TS1**. This indicate **1** and **2** are loosely bounded to **5** in **5-a-TS1** (217i cm^{-1}) in contrast with the compact assembly of **5-s-TS1** (323i cm^{-1}). Especially, there is no H-bonded interaction between N atom of **2** and thiourea of **5** in **5-a-TS1** and **5-a-TS2**. In step2, lengths of the forming N8-H7 and the breaking C6-H7 bonds are 1.06 and 1.89 Å in **5-s-TS2** (945i cm^{-1}); 1.13 and 1.64 Å in **5-a-TS2** (835i cm^{-1}). In **5-a-TS2**, not only the distance of N2-C3 (1.91 Å) is longer than that of **5-s-TS2** (1.89 Å), but also the C1-N2 bond elongates to 1.64 Å. This reveals that the interaction between **5** and **1** in **5-a-TS2** remains weaker even if the catalyst itself experiences a bigger change in structure.

The relationship among atoms directly involved in bond formation and dissociation could be exhibited visually by the highest occupied molecular orbital (HOMO) of transition states (right column of Fig. 3). In HOMO of **5-s-TS1**, the electropositive parts (+) of p orbital of C4 and C5 atoms overlap with each other to make a bonding interaction, which also exists among most of the adjacent atoms. The superposition turns to the electronegative parts (−) of p orbital and is dramatically reduced in HOMO of **5-a-TS1**. Combined with the surrounding anti bonding characters, the less favored C-C bond formation *via* **5-a-TS1** is rationalized. For **TS2**, H7 atom is located exactly at the node between two phases of the wave function, which corresponds to a typical HOMO shape of proton transfer. In **5-a-TS2**, there is a small superposition between s orbital of H7 and (+)p orbital of N8 as well as a big one between it and (−)p orbital of C6. In **5-s-TS2**, the former superposition is remarkably increased and the latter is decreased. It follows that the bonding interaction of N8-H7 is stronger in **5-s-TS2** than in **5-a-TS2**. Thereby the proton transfer from C6 to N8 is more readily *via* **s** path than **a** path.

Solvent Effect and Energetic Profiles: It is known that the solvent effect has a great impact on reactions involving ions. Since there is no ionic species in our system, no large

Table 2. Energy barriers, activation Gibbs free energies of two steps and ee values of the *aza*-MBH-type reaction with full catalyst **5** in solution phase

	gas		in xylene		in DMF	
	Ea	ΔG$^{\neq}$	Ea	ΔG$^{\neq}$	Ea	ΔG$^{\neq}$
s-step1	18.60	19.67	9.05	10.24	8.38	9.54
s-step2	23.28	24.83	13.82	15.07	13.03	14.26
a-step1	20.02	20.99	11.31	11.73	9.16	9.97
a-step2	26.16	27.64	16.55	17.68	13.73	14.59
ee			97.6%		27.2%	

discrepancy appears on the overall trend of the relative energy profiles in solution and gas phase. To research the effect of active site environment on the catalytic reaction, we choose the parameters of non-polar xylene and polar DMF to estimate the solvation energy of main intermediates and transition states. In general, the free energies of all optimized structures in solution phase are lower than those in gas phase. The decrease is larger in DMF than in xylene presumably owing to the stronger polarity of DMF than xylene. Seen from Table 2, the energy barriers and activation Gibbs free energies in solution phase are also reduced in the same tendency.
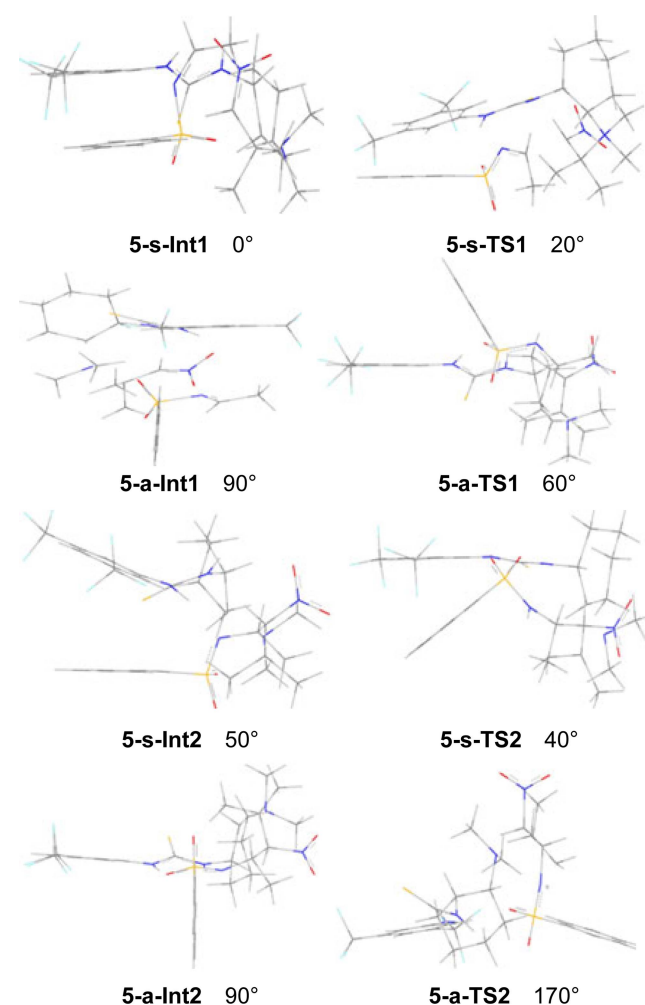
From Figure 2, the binary precursor **Int0** is stabilized by 3.13 kcal mol^{-1} with respect to isolated **5** and **1**. When the xylene was taken as solvent, in **s** path, the energy barriers of step1 and step2 are 9.05 and 13.82 kcal mol^{-1} (10.24 and 15.07 kcal mol^{-1} in free energy). In **a** path, the energy barriers are 11.31 and 16.55 kcal mol^{-1} (11.73 and 17.68 kcal mol^{-1} in free energy). The **s** path is determined to be more favorable than **a** path kinetically. Considering the enantioselectivity is dominated in rate-limiting step2, the enantiomer (3*S*,4*S*)-**3** generated in **s** path is the kinetic controlled product. From the perspective of thermodynamics, two paths are both endothermic in step1 (**s**: 2.17; **a**: 0.83 kcal mol^{-1}) and exothermic in step2 (**s**: −15.18; **a**: −13.35 kcal mol^{-1}). (3*S*,4*S*)-**3** is more stable than the product (3*S*,4*R*)-**3** of **a** path. Hence (3*S*,4*S*)-**3** is also preferential thermodynamically.[39]

Essence of Enantioselectivity. As Lewis base, the tertiary amine N enables the formation of a weak covalent bond between **5** and **1**. To study the role of weak covalent interaction on enantioselectivity of the reaction, we list some vital wiberg bond indices[40] in Table 3. BO value of C1-N2 bond has almost no change in step1. The BO value of N2-C3 in **5-s-TS1** (0.68) indicates a stronger interaction of **5** and **1** than that in **5-a-TS1** (0.57). Compared with the BO value of C4-C5 in **5-a-TS1** (0.33), the value in **5-s-TS1** (0.38) verifies the earlier C-C bond formation of **s** path than **a** path. In step2, BO value of C1-N2 bond is increased in **5-s-TS2** (0.83 → 0.90) while decreased in **5-a-TS2** (0.80 → 0.74). Although BO value of N2-C3 bond in **5-s-Int2** is smaller than that in **5-a-Int2**, it becomes bigger in **5-s-TS2** (0.47) than in **5-a-TS2** (0.42). BO values of C6-H7 and N8-H7 bonds in **5-s-TS2** (0.12, 0.61) demonstrate that the extent of C6-H7 bond dissociation and N8-H7 bond formation is

Table 3. Bond orders of major species with full catalyst **5** at B3LYP/6-311++G(d,p) level

Bond order	5-s-Int1	5-s-TS1	5-a-Int1	5-a-TS1
C1-N2	0.83	0.84	0.82	0.84
N2-C3	0.74	0.68	0.75	0.57
C4-C5		0.38		0.33
	5-s-Int2	**5-s-TS2**	**5-a-Int2**	**5-a-TS2**
C1-N2	0.83	0.90	0.80	0.74
N2-C3	0.68	0.47	0.74	0.42
C6-H7		0.12		0.26
N8-H7		0.61		0.47

much higher than that of **5-a-TS2** (0.26, 0.47). From the pre-intermediate to transition state, the smaller the BO value of N2-C3 bond changes, the easier the reaction proceeds.[39] Two steps of **s** path (0.06, 0.21) are both superior to those of **a** path (0.18, 0.32). In the activation of nitroalkene by tertiary amine *via* weak covalent bond, the weak covalent interaction not only stabilizes transition states in **s** path, but also orients

5-s-Int1 0°   **5-s-TS1** 20°

5-a-Int1 90°   **5-a-TS1** 60°

5-s-Int2 50°   **5-s-TS2** 40°

5-a-Int2 90°   **5-a-TS2** 170°

Figure 4. The π-π aromatic stacking interaction of related species in two steps of the *aza*-MBH-type reaction with full catalyst **5**. The approximate angles between two planes of aromatic ring are given in italic.

the reaction in **s** path with smaller variations of this bond.

From the steric perspective, we are intrigued by the impact of π-π stacking between aromatic rings of **5** and **2** on enantioselectivity (Fig. 4). The extent of π-π stacking relates directly to the efficient packing areas of aromatic rings, which is identical to the projected area proportional to the cosine value of angle between two planes. In a complex, the smaller angle corresponds to the larger extent of π-π stacking. A smaller change of the angle gives rise to an easier reaction process.[23] In **5-s-Int1**, two aromatic rings are almost parallel to each other. The aromatic ring of **5** tilts upward in **5-s-TS1** to form a 20° angel with the one of **2**. In contrast, two aromatic rings are vertical in **5-a-Int1**. The aromatic ring of **2** bends towards the one of **5** to form a 60° angel in **5-a-TS1**. The extent of π-π stacking in **5-s-Int2** (50°) is downhill from **5-s-TS1** and then somewhat increased in **5-s-TS2** (40°). As a comparison, the angle in **5-a-Int2** comes back to 90° *via* **5-a-TS1**. There is still little π-π stacking interaction in **5-a-TS2** ascribed to the aromatic rings stretching in opposite directions with a large angle of 170°. In the activation of N-tosylimine by aromatic ring *via* π-π stacking, the non-covalent interaction effectively stabilizes the species of **s** path and prefers **s** path with smaller changes of the efficient packing areas.

The enantiomeric excess (ee) of an isomer is measured by chiral column chromatography or NMR spectroscopy in experiment. Here, based on the calculation of rate constant (k) in transition state theory,[41] ee values (298 K) could be predicted employing the activation Gibbs free energies of rate-limiting step2 in different solution phase conditions[42] (Table 2). With xylene and DMF, the calculated ee values of (3*S*,4*S*)-**3** are 97.6% and 27.2%, respectively. The results are in accordance with experiment. It is known that the weak covalent interaction exerted by Lewis base and non-covalent interactions (H bonds, π-π stacking) would play their roles adequately in non-polar not polar environment. Therefore the ee value with xylene much higher than DMF confirms the cooperative effect of three types of interaction attributed by different units of catalyst on the domination of enantio-selectivity.

Conclusion

Our DFT calculations provide the first theoretical investigation on enantioselective *aza*-MBH-type reaction of nitroalkene and N-tosylimine catalyzed by thiourea-tertiary amine. The whole process contains two steps: nucleophilic addition of the nitroalkene-catalyst binary precursor to N-tosylimine; proton transfer from methyl of nitroalkene to the electronegative N of imine. Step2 is rate-limiting.

The research on real system with full catalyst elucidates the relationship between enantioselectivity and the structural properties of catalyst. Three functional groups of catalyst play different roles in the activation process. As Lewis base, the tertiary amine group activates nitroalkene *via* weak covalent bond. The weak covalent interaction orients the reaction in a major path with smaller variations of this bond.

On the other hand, the aromatic ring group activates N-tosylimine *via* π-π stacking. The non-covalent interaction selects the major path with smaller changes of the efficient packing areas. Thiourea group donates more compact H-bonded network in species of the major path. The enantio-selectivity is dominated by the cooperative effect of non-covalent and weak covalent interactions attributed by different units of catalyst. This conclusion is supported by the calculated ee values in non-polar xylene (97.6%) much higher than that in polar DMF (27.2%).

References

1. Li, C. J. *Acc. Chem. Res.* **2009**, *42*, 335.
2. Langer, P. *Angew. Chem. Int. Ed.* **2000**, *39*, 3049.
3. Masson, G.; Housseman, C.; Zhu, J. *Angew. Chem. Int. Ed.* **2007**, *46*, 4614.
4. Kataoka, T.; Kinoshita, H. *Eur. J. Org. Chem.* **2005**, 45.
5. Shi, Y. L.; Shi, M. *Eur. J. Org. Chem.* **2007**, *18*, 2905.
6. Pellissier, H. *Tetrahedron* **2006**, *62*, 2143.
7. Friestad, G. K.; Mathies, A. K. *Tetrahedron* **2007**, *63*, 2541.
8. Kraft, M. E.; Haxell, T. F. N.; Seibert, K. A.; Abboud, K. A. *J. Am. Chem. Soc.* **2006**, *128*, 4174.
9. Deb, I.; Dadwal, M.; Mobin, S. M.; Namboothiri, I. N. N. *Org. Lett.* **2006**, *8*, 1201.
10. Dadwal, M.; Mobin, S. M.; Namboothiri, I. N. N. *Org. Biomol. Chem.* **2006**, *4*, 2525.
11. Kraft, M. E.; Wright, J. A. *Chem. Commun.* **2006**, 2977.
12. Pohmakotr, M.; Thamapipol, S.; Tuchinda, P.; Prabpai, S.; Kongsaeree, P.; Reutrakul, V. *J. Org. Chem.* **2007**, *72*, 5418.
13. Wadhwa, K.; Chintareddy, V. R.; Verkade, J. G. *J. Org. Chem.* **2009**, *74*, 6681.
14. Reynolds, T. E.; Binkley, M. S.; Scheidt, K. A. *Org. Lett.* **2008**, *10*, 5227.
15. Zhao, G. L.; Shi, M. *Org. Biomol. Chem.* **2005**, *3*, 3686.

16. Maity, P.; Lepore, S. D. *J. Am. Chem. Soc.* **2009**, *131*, 4196.
17. Wang, X.; Chen, Y. F.; Niu, L. F.; Xu, P. F. *Org. Lett.* **2009**, *11*, 3310.
18. Singh, V.; Batra, S. *Tetrahedron* **2008**, *64*, 4511.
19. Siegel, J. B.; Zanghellini, A.; Lovick, H. M.; Kiss, G.; Lambert, A. R.; Clair, J. L. St.; Gallaher, J. L.; Hilvert, D.; Gelb, M. H.; Stoddard, B. L.; Houk, K. N.; Michael, F. E.; Baker, D. *Science* **2010**, *329*, 309.
20. Houk, K. N.; Cheong, P. H. Y. *Nature* **2008**, *455*, 309.
21. Sieffert, N.; Bühl, M.; Gaigeot, M. P.; Morrison, C. A. *J. Chem. Theory Comput.* **2013**, *9*, 106.
22. Hujo, W.; Grimme, S. *J. Chem. Theory Comput.* **2013**, *9*, 308.
23. Lu, N.; Meng, L.; Chen, D. Z.; Zhang, G. Q. *J. Phys. Chem. A* **2012**, *116*, 670.
24. Frisch, M. J. *et al. Gaussian 09*, Revision B.01; Gaussian, Inc. (Wallingford, CT, 2009).
25. Becke, A. D. *J. Chem. Phys.* **1993**, *98*, 5648.
26. Becke, A. D. *J. Chem. Phys.* **1996**, *104*, 1040.
27. Lee, C.; Yang, W.; Parr, R. G. *Phys. Rev. B* **1988**, *37*, 785.
28. Tapia, O. *J. Math. Chem.* **1992**, *10*, 139.
29. Tomasi, J.; Persico, M. *Chem. Rev.* **1994**, *94*, 2027.
30. Simkin, B. Y.; Sheikhet, I. *Quantum Chemical and Statistical Theory of Solutions - A Computational Approach*; Ellis Horwood: London, 1995.
31. Tomasi, J.; Mennucci, B.; Cammi, R. *Chem. Rev.* **2005**, *105*, 2999.
32. Marenich, A. V.; Cramer, C. J.; Truhlar, D. G. *J. Phys. Chem. B* **2009**, *113*, 327.
33. Zhu, R. X.; Zhang, D. J.; Wu, J.; Liu, C. B. *Tetrahedron: Asymmetry* **2006**, *17*, 1161.
34. Zhao, Y.; Lynch, B. J.; Truhlar, D. G. *J. Phys. Chem. A* **2004**, *108*, 2715.
35. Boys, S. F.; Bernardi, F. *Mol. Phys.* **1970**, *19*, 553.
36. Reed, A. E.; Weinstock, R. B.; Weinhold, F. *J. Chem. Phys.* **1985**, *83*, 735.
37. Reed, A. E.; Curtiss, L. A.; Weinhold, F. *Chem. Rev.* **1988**, *88*, 899.
38. Lloyd, D. R. *Chem. Phys. Lett.* **2000**, *323*, 198.
39. Lu, N.; Meng, L.; Chen, D. Z.; Zhang, G. Q. *J. Mol. Catal. A: Chem.* **2011**, *339*, 99.
40. Wiberg, K. B. *Tetrahedron* **1968**, *24*, 1083.
41. Truhlar, D. G.; Garrett, B. C.; Klippenstein, S. J. *J. Phys. Chem.* **1996**, *100*, 12771.
42. Chen, D. Z.; Lu, N.; Zhang, G. Q.; Mi, S. Z. *Tetrahedron: Asymmetry* **2009**, *20*, 1365.